동력시스템공학회지 제29권 제3호 pp. 35-46 2025년 6월 ISSN 2713-8429(Print) ISSN 2713-8437(Online)
Journal of Power System Engineering https://doi.org/10.9726/kspse.2025.29.3.035
Vol. 29, No. 3, pp. 35-46, June 2025

Characterization of the EIS Diffusion Region in Cylindrical Lithium–Ion Batteries as a Function of Temperature and State of Charge

Jin-Yong Bae*†

(Received 29 May 2025, Revision received 27 June 2025, Accepted 27 June 2025)

Abstract : This study investigates the effect of temperature and state of charge (SoC) on the electrochemical impedance characteristics of the diffusion region in cylindrical lithium-ion batteries. The increasing occurrence of fires and explosions related to lithium-ion batteries, which are widely employed in energy storage applications, underscores the necessity for enhancing their inherent safety features. Consequently, electrochemical impedance spectroscopy (EIS) is employed in the frequency range of 1 kHz to 0.1 Hz as an analytical technique for energy storage systems. Reflected wave analysis is then utilized to monitor internal impedance variations in the lithium-ion battery. Variations in the low-frequency diffusion region are examined in terms of their dependence on the structural and material characteristics of the diffusion layer and electroactive components of the lithium-ion battery. This study employs a 3000 mAh-class NCA ($Li[Ni,Co,Al]O_2$) 18650 lithium-ion battery, which is widely used in energy storage systems, electric scooters, electric motorcycles, electric kickboards, and compact electric vehicles. Depending on the characteristics of the diffusion layer and electroactive material, lithium-ion batteries exhibit three distinct diffusion behaviors in the low-frequency diffusion region: (1) finite-space Warburg (FSW), (2) finite-length Warburg (FLW), and (3) constant phase element (CPE). Among these, the finite-space Warburg (FSW) element is not observed, while the constant phase element (CPE) and finite-length Warburg (FLW) behaviors are observed in two cases. Furthermore, in cylindrical lithium-ion batteries, the low-frequency diffusion region—where temperature and state of charge (SoC) influence performance—can be categorized into four types: (1) Warburg diffusion, (2) semi-spherical diffusion, (3) bounded diffusion, and (4) semi-cylindrical diffusion.

Key Words : Electrochemical Impedance Spectroscopy, Finite-Space Warburg, Finite-Length Warburg, Constant Phase Element, Warburg Diffusion

1. Introduction

Due to recent incidents of fires and explosions, there is an urgent need for fundamental safety improvements in lithium-ion batteries, which are widely used as energy storage devices in electric vehicles, personal mobility devices, mobile phones, and various electronic products.[1,2)]

Lithium-ion batteries facilitate the efficient utilization of sustainable electric energy and support the active integration of renewable energy sources such as solar and wind power.[3,4)]

Battery management systems (BMS) for the stable operation of energy storage devices are the subject

*† Jin-Yong Bae(https://orcid.org/0000-0003-0554-3621) : Professor,
Department of Electrical Engineering, Suwon University.
E-mail : bjy@suwon.ac.kr, Tel : 031-220-2300

of active research.[5,6)]

The study conducted by Junqiu Li et al.[7)] involved a thermal characteristic analysis and impedance-based thermal modeling of lithium-ion batteries in an overcharge state, with the aim of assessing both thermal safety and the accuracy of thermal modeling.

Peng Peng et al.[8)] performed a numerical analysis of the thermal stability of lithium-ion batteries, focusing on the cathode material. To experimentally validate these findings for electric vehicle batteries, Jan Kleiner et al.[9)] developed a thermal model for prismatic lithium-ion batteries.

Karden E. et al.[10)] presented a frequency- domain methodology for the dynamic simulation of electrochemical power sources. M. Oldenburger et al.[11)] investigated the low-frequency Warburg impedance in lithium-ion batteries.

This study investigates the effects of temperature and SoC on the EIS characteristics within the diffusion region of cylindrical lithium-ion batteries. Furthermore, to evaluate internal impedance variations based on reflected wave analysis, a range of input frequencies from 1 kHz to 0.1 Hz is applied to the battery.

Depending on the properties of the diffusion layer and electroactive materials, lithium-ion batteries exhibit three distinct diffusion pathways in the low-frequency diffusion region: (1) FSW, (2) FLW, and (3) CPE. The results indicate that cylindrical lithium-ion batteries exhibit FLW behavior under abnormal conditions—specifically, at temperatures below -5℃ and a SoC of 0%. In contrast, under normal operating conditions, when the diffusion layer and electroactive material properties are sufficient, the batteries demonstrate CPE characteristics. Depending on variations in temperature and SoC, the FLW behavior in lithium-ion batteries can manifest in three distinct forms: (1) BD, (2) SSD, and (3) SCD.

2. Diffusion characteristics in the low frequency region of cylindrical lithium-ion batteries

The complex-plane plot of the EIS data for a cylindrical lithium-ion battery is illustrated in Fig. 1.[18)]

As shown in Fig. 1, the series inductance (L_s) is manifested in the high-frequency region $(f_{\max})$, while the series resistance (R_s) is identified at the intersection of the real axis and the impedance spectrum trajectory at high frequencies.

The charge transfer process at the solid electrolyte interphase (SEI), characterized by the film resistance (R_{SEI}) and the constant phase element (Q_{SEI}, α_{SEI}), is represented by a small semicircle in the impedance spectrum.

When the charge transport across the electrode–electrolyte interface exceeds the capacity for charge storage, a pronounced semicircular arc emerges in the impedance spectrum. This feature is associated with the charge transfer resistance (R_{ct}) in parallel with a constant phase element (Q_{SEI}, α_{SEI}) representing the interfacial double-layer behavior.

The Warburg impedance (Z_W), indicative of ion diffusion within the electrolyte, reflects lithium-ion transport behavior and is influenced by the structural characteristics of the diffusion layer and the nature

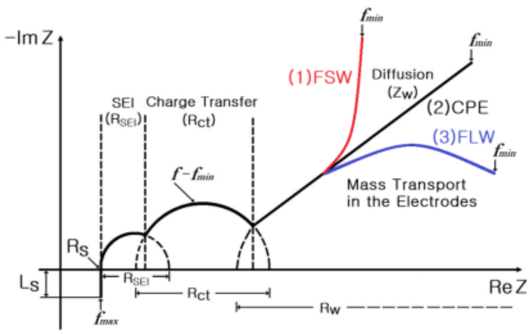

Fig. 1 EIS of cylindrical lithium-ion battery

Table 1 Diffusion Equations and Nyquist Impedance Diagrams at Low Frequencies

Division	Diffusion Impedance Equation	Nyquist Impedance Diagram
WD (45° Tilt)	$Z_W = R_\omega \cdot \frac{1}{\sqrt{j\omega}}$	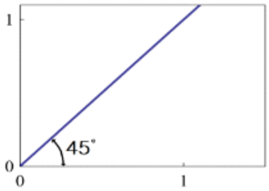
SSD	$Z_W = R_\omega \cdot \frac{1}{1+\sqrt{j\omega}}$	
BD	$Z_W = R_\omega \cdot \frac{1}{\sqrt{j\omega}} \tanh(\sqrt{j\omega})$	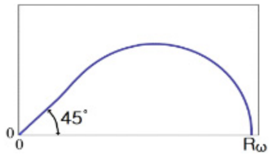
SCD	$Z_W = R_\omega \cdot \frac{1}{\sqrt{j\omega}} \frac{K_0(j\omega)}{K_1(j\omega)}$	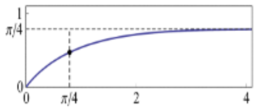

of the electroactive material, manifesting in three distinct regimes.

In the case of the finite-space Warburg (FSW) element, both the diffusion layer and the amount of electroactive material were limited. For the finite-length Warburg (FLW) element, although the diffusion layer remained limited, the amount of electroactive material was sufficient. In contrast, the constant phase element (CPE) exhibited sufficient diffusion layer and electroactive material, with both properties further enhanced by a 45° tilt angle.

Fig. 2 displays the complex plan view of the impedance spectrum at 100% and 50% SoC of a 3000 mA class 18650 cylindrical lithium-ion battery for temperature ranging from 40℃ to -20℃ in 15℃ increments.

Table 1 summarizes the diffusion equations and corresponding Nyquist impedance diagrams at low frequencies observed in lithium-ion batteries.

Here,

Z_W : diffusion impedance

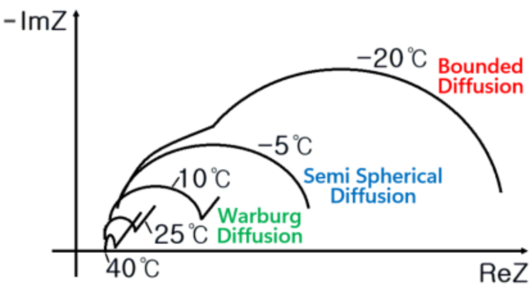

Fig. 2 EIS curve at 100% and 50% SoC form 40℃ to -20℃

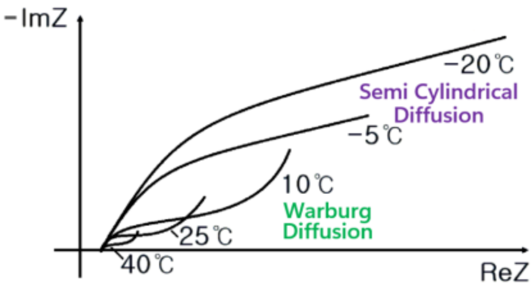

Fig. 3 EIS curve from 40℃ to -20℃ under 0% SoC

R_ω : diffusion resistance (horizontal axis value at the point where the imaginary part has a minimum value)

K_0, K_1: coefficient for SCD

When the diffusion layer and electroactive material are sufficiently available, a characteristic WD response—manifested as a 45° slope in the Nyquist plot—emerges in the low-frequency region of the impedance spectrum. This behavior is typically observed under conditions where the SoC exceeds 50% and the temperature is above 10℃ in lithium-ion batteries.

Below 40℃, the charge transfer resistance is characterized by a relatively small semicircle, while the Warburg impedance extends, indicating enhanced diffusion behavior. However, as the temperature decreases further, the Warburg region becomes shorter, and the charge transfer resistance increases, resulting in a broader semicircle in the Nyquist plot.

At -5℃, a pronounced semi-spherical diffusion (SSD) region appears in the impedance spectrum, while the WD element, typically characterized by a 45° slope, is entirely absent. As the temperature further decreases to -20℃, the size of the BD region increases significantly.

Consequently, when the SoC is sufficiently high, the CPE behavior transitions to FLW behavior as the temperature decreases.

As shown in Fig. 2, the condition of the electrolyte changes markedly, and the resistance of the diffusion region increases sharply below -5℃ when the temperature is reduced at SoC of 100% or 50%, both exceeding a critical threshold. At -20℃, the diffusion region displays a significantly enlarged semicircle in the impedance spectrum, attributed to the increased diffusion resistance. When the diffusion layer is limited while the electroactive material remains sufficient, the charge transfer resistance (R_{ct}) of the electrode increases, and the double-layer capacitance (Q_{SEI}, α_{SEI}) manifests as a semicircular arc in the impedance spectrum.

As shown in Fig. 3, at 0% SoC, Warburg impedance typically appears only when both the diffusion layer and the electroactive material are sufficiently present, and the temperature exceeds 10℃.

This condition is characterized by the presence of a sufficiently developed diffusion layer and a limited quantity of electroactive material.

Below -5℃, a SCD region emerges, while the WD component is entirely absent. At -20°C, the SCD region becomes significantly more pronounced, indicating a further increase in diffusion-related resistance. The variation in the diffusion region as the temperature decreases from 40℃ to -20℃ is summarized as follows.

When the SoC is sufficient, such as at 100% and 50% SoC, the observed sequence follows WD to SSD, and then to BD. However, when the SoC is insufficient, specifically at 0% SoC, the sequence progresses from WD to SCD.

Fig. 4 illustrates the Nyquist plot of EIS for a cylindrical lithium-ion battery at SoC above 10℃.

A semicircular arc corresponding to charge transfer is observed at 100% and 50% SoC, where the SoC exceeds a certain threshold.

However, at 0% SoC, the absence of electroactive material hinders charge transfer. In the low-frequency

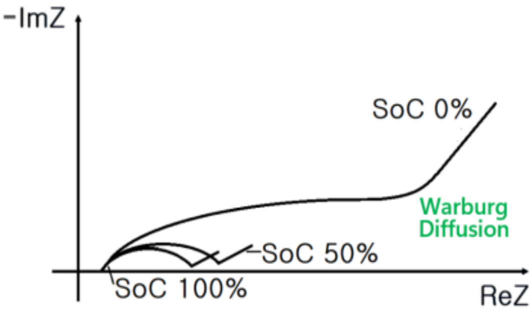

Fig. 4 EIS curve over 10℃ from 0% SoC to 100% SoC

range, Warburg impedance characteristics are observed, manifested by a 45° slope, indicating diffusion-controlled behavior.

Fig. 5 presents the Nyquist plot of EIS for the cylindrical lithium-ion battery at -5℃, as a function of SoC.

Below -5℃, the diffusion layer becomes limited, and a FLW region is observed in the impedance spectrum.

A SSD region is observed at 100% and 50% SoC, whereas a SCD region appears at 0% SoC.

Fig. 6 displays the Nyquist plot of EIS for the cylindrical lithium-ion battery at -20℃, as a function of SoC.

Below -20℃, the diffusion layer becomes limited, and a FLW region is observed. At 100% and 50% SoC, a BD region appears, whereas at 0% SoC, a SCD region is observed.

The variation in the diffusion region with decreasing SoC from 100% to 0% is summarized as follows.

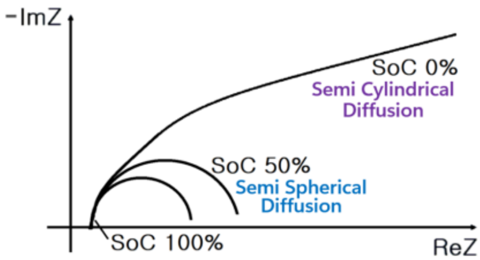

Fig. 5 EIS Curve at -5℃ from 0% SoC to 100% SoC

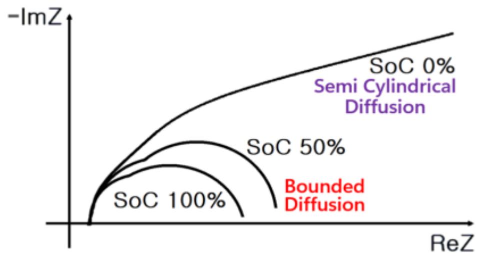

Fig. 6 EIS Curve at -20℃ from 0% SoC to 100% SoC

At temperatures of 40℃, 25℃, and 10℃, the process corresponds to WD. When the temperature decreases to -5℃, the sequence progresses from SSD to SCD. Further lowering the temperature to -20℃ results in the transition from BD to SCD.

The equivalent impedance of the lithium-ion battery can be quantitatively expressed by Equation (1) as follows:

$$Z(w) = jwL + R_S + \frac{R_{SEI}}{1 + R_{SEI} \cdot Q_{SEI}(jw)^{\alpha_{SEI}}} + \frac{R_{CT}}{1 + R_{CT} \cdot Q_{dl}(jw)^{\alpha_{dl}}} \tag{1}$$

When charge transfer occurs at the electrode interface, the electrode resistance and double-layer capacitance observed at higher states of charge are absent at 0% SoC. This behavior can be mathematically expressed as follows:

$$Z(w) = jwL + R_S + \frac{R_{SEI}}{1 + R_{SEI} \cdot Q_{SEI}(jw)^{\alpha SEI}} + \frac{1}{Q(jw)^n} \tag{2}$$

Equation (3) presents the impedance of the diffusion region for a 3000 mA-class 18650 cylindrical lithium-ion battery. Based on this equation, the diffusion impedance can be classified into WD, SSD, BD, and SCD types.

$$\begin{aligned} Z_W &= \frac{1}{Q(jw)^n} && (3) \\ &= R_\omega \cdot \frac{1}{\sqrt{j\omega}} && : \text{WD} \\ &= R_\omega \cdot \frac{1}{1+\sqrt{j\omega}} && : \text{SSD} \\ &= R_\omega \cdot \frac{1}{\sqrt{j\omega}} \tanh(\sqrt{j\omega}) && : \text{BD} \\ &= R_\omega \cdot \frac{1}{\sqrt{j\omega}} \frac{K_0(j\omega)}{K_1(j\omega)} && : \text{SCD} \end{aligned}$$

3. Experimental Results

Fig. 7 illustrates the experimental setup used for measuring the impedance of lithium-ion batteries.

The properties of a single cell of the cylindrical lithium-ion battery were examined.

The analysis was conducted by considering a range of parameter values. Specifically, the SoC was evaluated at three levels: 100%, 50%, and 0%. In addition, the temperature conditions included 40℃, 25℃, 10℃, -5℃, and -20℃, to account for a wide spectrum of thermal environments.

The series inductance (L_s), series resistance (R_s), and parallel resistance (R_p) are influenced by the electrolyte properties and battery structure. Furthermore, the diffusion area impedance (Z_W) at low frequencies is strongly correlated with the electrolyte's low frequency properties, and the electric double layer is associated with the parallel capacitor (C_p).

The cell voltage of the cylindrical lithium-ion battery was 4.2 V at 100% SoC. Fig. 9 presents the impedance spectrum of the cylindrical lithium-ion battery at 100% SoC under varying temperatures.

At 100% SoC, the cylindrical lithium-ion battery exhibits a resistance value between 17.0598 and 276.9609 mΩ.

In Fig. 8, the R_s, R_p, and L_s values increase with decreasing temperature.

Particularly, at -20℃, R_p rapidly increases, implying that the battery performance rapidly decreases at temperatures below -5℃.

Under 100% SoC, CPE transforms to FLW as the temperature decreases. Furthermore, at 100% SoC, the following transformation was experimentally observed with decreasing temperature : WD ‣ SSD ‣ BD.

(a) Experimental equipment

(b) Frequency injection device and chamber

(c) 18650 Lithium-ion battery (Samsung SDI, 3000 mAh)

Fig. 7 Experimental equipment for measuring the impedance of lithium-ion batteries

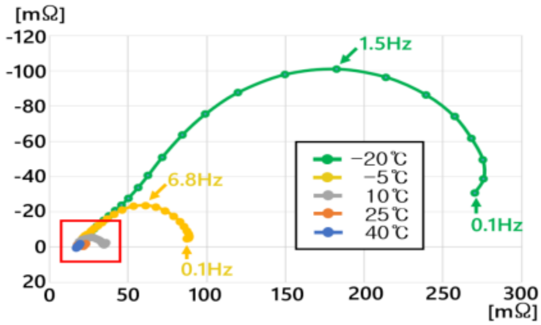

Fig. 8 Impedance spectrum of the cylindrical lithium-ion battery at 100% SoC under different temperatures

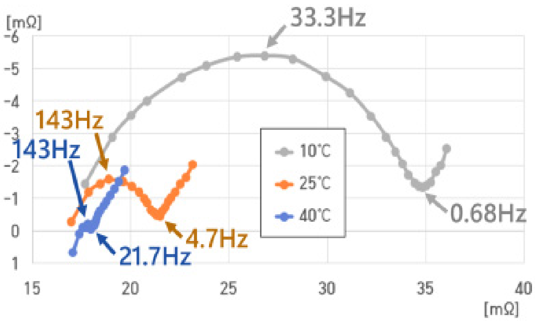

Fig. 9 Impedance spectrum at 40℃, 25℃, and 10℃ under 100% SoC for the cylindrical lithium-ion battery

Table 2 R_s, R_p, C_p, and L_s (100% SoC)

Division	100% SoC
40°C	R_s = 17.3908 mΩ, R_p = 0.5737 mΩ C_p = 0.0625 F, L_s = 2.7678 mH
25°C	R_s = 17.5424 mΩ, R_p = 3.9478 mΩ C_p = 0.0337 F, L_s = 2.7920 mH
10°C	R_s = 17.6737 mΩ, R_p = 17.1868 mΩ C_p = 0.1247 F, L_s = 2.8129 mH
-5°C	R_s = 19.1924 mΩ, R_p = 68.0877 mΩ C_p = 0.3827 F, L_s = 3.0546 mH
-20°C	R_s = 23.4937 mΩ, R_p = 252.3713 mΩ C_p = 0.5820 F, L_s = 3.7391 mH

Table 3 R_s, R_p, C_p, and L_s (100% SoC)

Division	50% SoC
40°C	R_s = 17.4221 mΩ, R_p = 1.6107 mΩ C_p = 0.0601 F, L_s = 2.7728 mH
25°C	R_s = 17.5368 mΩ, R_p = 5.6832 mΩ C_p = 0.0543 F, L_s = 2.7911 mH
10°C	R_s = 18.7598 mΩ, R_p = 19.2028 mΩ C_p = 0.1190 F, L_s = 2.9857 mH
-5°C	R_s = 20.4916 mΩ, R_p = 93.2054 mΩ C_p = 0.4597 F, L_s = 3.2613 mH
-20°C	R_s = 23.9596 mΩ, R_p = 386.7496 mΩ C_p = 0.6367 F, L_s = 3.6541 mH

Fig. 9 depicts an extended impedance spectrum waveform under 100% SoC at 40℃, 25℃, and 10℃.

Table 2 summarizes the parameters R_s, R_p, C_p, and L_s measured at 100% SoC.

Fig. 9 illustrates that WD occurs below 21.7 Hz at 40℃, 3.3 Hz at 25°C, and 0.68 Hz at 10℃.

At -5℃, WD is absent, but SSD is present. Moreover, at -20℃, WD is absent but BD is present. The cell voltage of the cylindrical lithium-ion battery at 50% SoC was 3.65 V.

Fig. 10 exhibits the impedance spectra for the cylindrical lithium-ion battery at 50% SoC under varying temperatures.

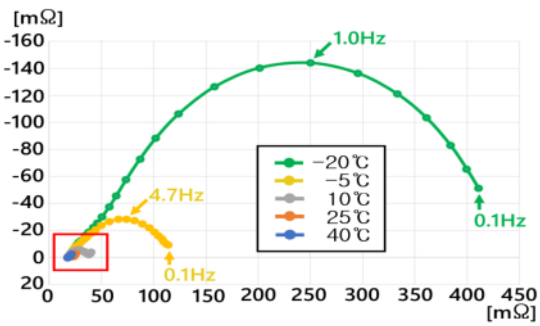

Fig. 10 Impedance spectrum of the cylindrical lithium-ion battery at 50% SoC under different temperatures

As depicted in Fig. 10, the resistance value of the cylindrical lithium-ion battery at 50% SoC ranges from 17.4221 to 410.7092 mΩ.

As shown in Fig. 10, R_s, R_p, and L_s decrease with increasing and decreasing temperatures. Particularly, R_p quickly increases at -20℃, suggesting that the battery performance quickly deteriorates below -5℃.

Table 3 presents the values of R_s, R_p, C_p, and L_s at 50% SoC.

At 50% SoC, CPE transforms to FLW with decreasing temperature. At 50% SoC, the following transformation was experimentally observed with decreasing temperature : WD ‣ SSD ‣ BD.

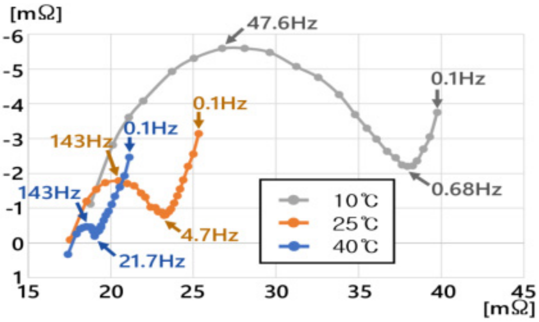

Fig. 11 Impedance spectrum at 40℃, 25℃, and 10℃ under 50% SoC for the cylindrical lithium-ion battery

Fig. 11 displays an enlarged impedance spectrum waveform at 50% SoC under 40℃, 25℃, and 10℃. In Fig. 11, WD occurs below 21.7 Hz at 40℃, below 4.7 Hz at 25℃, and below 0.68 Hz at 10℃.

At -5℃, WD is absent, but SSD is present. At -20℃, WD is absent but BD is present.

The cell voltage of the cylindrical lithium-ion battery at 0% SoC was 2.5 V. Fig. 12 presents the impedance spectrum for the cylindrical lithium-ion battery at 0% SoC under different temperatures.

Fig. 12 shows that the cylindrical lithium-ion battery at 0% SoC has a resistance value between 17.5448 and 899.8490 mΩ.

In Fig. 12, the R_s, R_p, and L_s values increase with decreasing temperature. However, the C_p value decreases with the temperature, in contrast to that

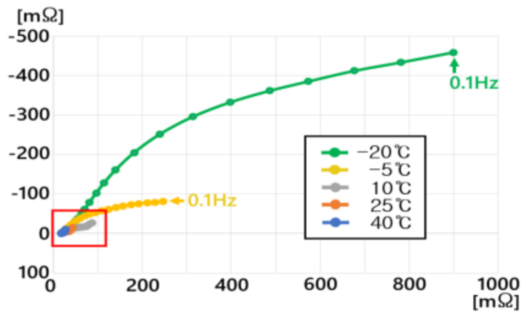

Fig. 12 Impedance spectrum of the cylindrical lithium -ion battery at 0% SoC under different temperatures

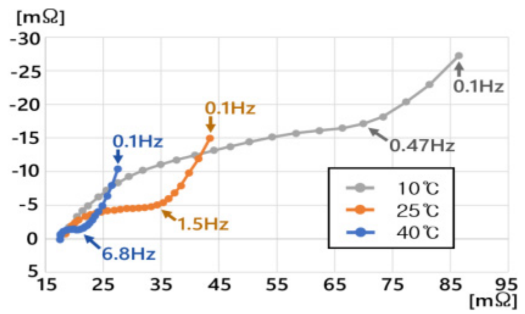

Fig. 13 Impedance spectrum at 40℃, 25℃, and 10℃ under 0% SoC for the cylindrical lithium-ion battery

Table 4 R_s, R_p, C_p, and L_s (0% SoC)

Division	0% SoC
40℃	R_s = 17.5448 mΩ, R_p = 3.1019 mΩ C_p = 57.8878 F, L_s = 2.7923 mH
25℃	R_s = 18.4584 mΩ, R_p = 13.7520 mΩ C_p = 36.6656 F, L_s = 2.9378 mH
10℃	R_s = 19.0909 mΩ, R_p = 50.8780 mΩ C_p = 18.4127 F, L_s = 3.0384 mH
-5℃	R_s = 20.6691 mΩ, R_p = 225.2969 mΩ C_p = 6.4698 F, L_s = 3.2856 mH
-20℃	R_s = 25.2552 mΩ, R_p = 874.5938 mΩ C_p = 1.7687 F, L_s = 4.0195 mH

under 100% and 50% SoC. This is because 0 Hz isthe frequency at which the imaginary axis value, -ImZ, reaches its maximum.

Particularly, at -20℃, R_p rapidly increases, implying that the battery performance rapidly worsens at temperatures below -5℃.

Under 0% SoC, CPE transforms to FLW as the temperature decreases. At 0% SoC, the following transformation was experimentally observed with decreasing temperature : WD ‣ SCD.

Table 4 shows the electrical parameters R_s, R_p, C_p, and L_s obtained at 0% SoC.

Fig. 13 shows a large representation of the impedance spectrum waveform in Fig. 12 under 0% SoC and 40°C, 25℃, and 10℃.

Fig. 13 illustrates that WD occurs below 6.8 Hz at 40℃, 1.5 Hz at 25℃, and 0.47 Hz at 10℃.

At -5℃ and -20℃, WD is absent but SCD is present.

At 100% SoC, R_s and R_p were small and C_p was also very small, verifying that the impedance spectrum curve progressed along the X-axis overall.

R_s and R_p at 50% SoC were somewhat greater than those at 100% SoC. At 0% SoC, R_s and C_p significantly increased along the Y-axis with a slope of about 45°.

Fig. 14 compares the performance of the cylindrical lithium-ion battery at 0%, 50%, and 100% SoC under 40°C. The resistance value of the battery ranges from 17.0598 to 27.4937 mΩ.

Table 5 summarizes the parameters R_s, R_p, C_p, and L_s measured at 40℃.

At 40℃, R_s, R_p, and L_s decreased with increasing SoC, and vice versa.

However, at 0% SoC, C_p rapidly increased compared to that at 100% and 50% SoC, signifying that C_p increased with Z_W for 0% SoC.

At 40℃, the diffusion area is a low-frequency characteristic that manifests as CPE = WD, as proved experimentally. Fig. 14 shows that WD occurs below 6.8 Hz at 0% SoC and below 21.7 Hz at 100% and 50% SoC.

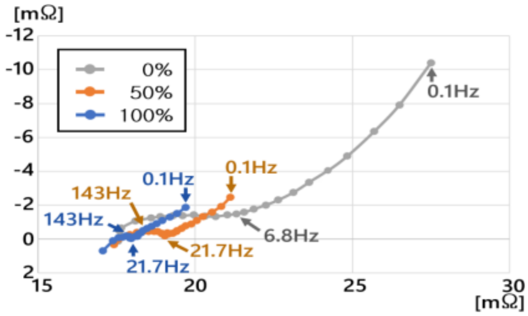

Fig. 14 Impedance spectrum of the cylindrical lithium-ion battery at different SoCs under 40℃

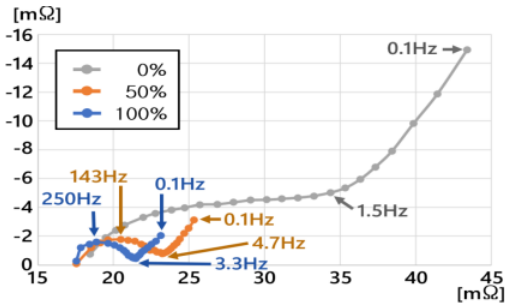

Fig. 15 Impedance spectrum of the cylindrical lithium -ion battery at different SoCs under 25℃

Table 5 R_s, R_p, C_p, and L_s (40℃)

Division	40℃
100% SoC	R_s = 17.3908 mΩ, R_p = 0.5737 mΩ C_p = 0.0625 F, L_s = 2.7678 mH
50% SoC	R_s = 17.4221 mΩ, R_p = 1.6107 mΩ C_p = 0.0601 F, L_s = 2.7728 mH
0% SoC	R_s = 17.5448 mΩ, R_p = 3.1019 mΩ C_p = 57.8878 F, L_s = 2.7923 mH

Table 6 R_s, R_p, C_p, and L_s (25℃)

Division	25°C
100% SoC	R_s = 17.5424 mΩ, R_p = 3.9478 mΩ C_p = 0.0337 F, L_s = 2.7920 mH
50% SoC	R_s = 17.5368 mΩ, R_p = 5.6832 mΩ C_p = 0.0543 F, L_s = 2.7911 mH
0% SoC	R_s = 18.4584 mΩ, R_p = 13.7520 mΩ C_p = 36.6656 F, L_s = 2.9378 mH

Fig. 15 compares the impedance spectrum results for the cylindrical lithium-ion battery at 0%, 50%, and 100% SoC under 25℃. The battery's resistance value varies between 17.5424 and 43.4072 mΩ.

Fig. 15 shows that at 25℃, R_s, R_p, C_p, and L_s decrease with increasing SoC. However, at 0% SoC, C_p rapidly increased compared to that at 100% and 50% SoC. Thus, at 0% SoC, C_p increased with Z_W.

The diffusion area, a low-frequency characteristic at 25℃, was experimentally verified to manifest as CPE = WD.

Table 6 presents the values of R_s, R_p, C_p, and L_s at 25℃.

As depicted in Fig. 15, WD occurs below 3.3 Hz at 100% SoC, below 4.7 Hz at 50% SoC, and below 1.5 Hz at 0% SoC.

Fig. 16 compares the impedance spectrum results for the cylindrical lithium-ion battery at 0%, 50%, and 100% SoC under 10℃. The resistance value of the battery ranges from 17.6737 to 86.4376 mΩ.

R_s, R_p, and L_s decreased with increasing SoC, and vice versa. C_p increased quicker at 0% SoC than that at 100% and 50% SoC. Consequently, C_p increased with Z_W at 0% SoC.

The diffusion area, a low-frequency feature, was experimentally verified to appear as CPE = WD at 10℃. Fig. 16 shows that WD occurs below 0.47 Hz at 0% SoC and below 0.68 Hz at 100% and 50% SoC.

Fig. 17 compares the impedance spectrum results for the cylindrical lithium-ion battery at 0%, 50%, and 100% SoC under -5℃. The battery's resistance value varies between 19.1924 and 245.9957 mΩ.

Table 7 shows the electrical parameters R_s, R_p, C_p, and L_s obtained at 10°C.

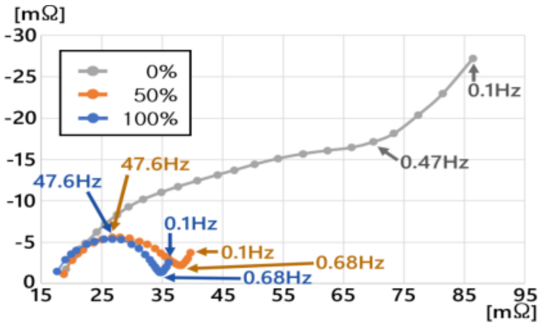

Fig. 16 Impedance spectrum of the cylindrical lithium-ion battery at different SoCs under 10℃

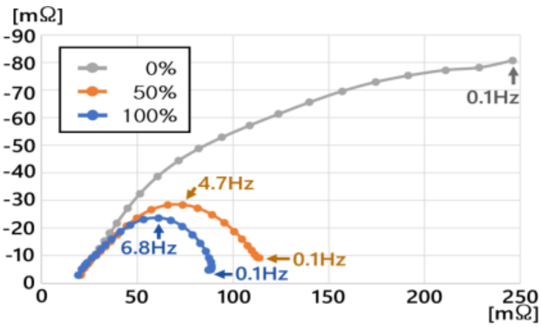

Fig. 17 Impedance spectrum of the cylindrical lithium-ion battery at different SoCs under -5℃

Table 7 R_s, R_p, C_p, and L_s (10℃)

Division	10°C
100% SoC	R_s = 17.6737 mΩ, R_p = 17.1868 mΩ C_p = 0.1247 F, L_s = 2.8129 mH
50% SoC	R_s = 18.7598 mΩ, R_p = 19.2028 mΩ C_p = 0.1190 F, L_s = 2.9857 mH
0% SoC	R_s = 19.0909 mΩ, R_p = 50.8780 mΩ C_p = 18.4127 F, L_s = 3.0384 mH

Table 8 R_s, R_p, C_p, and L_s (-5℃)

Division	-5°C
100% SoC	R_s = 19.1924 mΩ, R_p = 68.0877 mΩ C_p = 0.3827 F, L_s = 3.0546 mH
50% SoC	R_s = 20.4916 mΩ, R_p = 93.2054 mΩ C_p = 0.4597 F, L_s = 3.2613 mH
0% SoC	R_s = 20.6691 mΩ, R_p = 225.2969 mΩ C_p = 6.4698 F, L_s = 3.2856 mH

R_s, R_p, C_p, and L_s decreased with increasing SoC, and vice versa At 0% SoC, C_p rapidly increased compared to that at 100% and 50% SoC. Thus, at 0% SoC, C_p increased with Z_W.

Experimental results confirmed that the diffusion region, exhibiting a low-frequency characteristic at -5℃, corresponds to the FLW phenomenon as shown in Fig. 17.

As the SoC decreased from 100%, 50%, to 0%, the transformation from SSD to SCD occurred.

The values of R_s, R_p, C_p, and L_s at -5℃ are listed in Table 8.

Fig. 18 compares the impedance spectrum results for the cylindrical lithium-ion battery at 0%, 50%, and 100% SoC under -20℃. The resistance value of the battery ranges from 23.4937 to 899.8488 mΩ .

Specifically, R_s, R_p, C_p, and L_s decreased with increasing SoC, and vice versa. At 0% SoC, C_p

rapidly increased compared to that at 100% and 50% SoC. Thus, at 0% SoC, C_p increased with Z_W.

-20℃ SoC, the corresponding R_s, R_p, C_p, and L_s values are provided in Table 9.

The diffusion region, characterized by a low-frequency response at -20℃, was experimentally confirmed to manifest as FLW, as shown in Fig. 18.

As SoC decreased from 100%, 50%, to 0%, transformation from SSD to BD occurred.

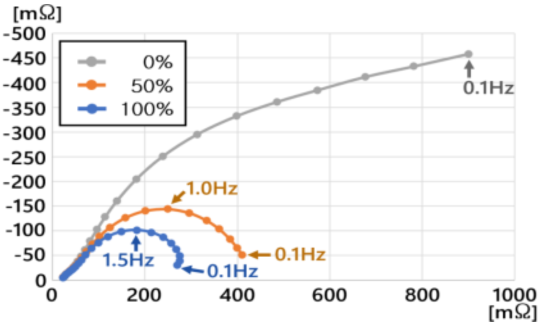

Fig. 18 Impedance spectrum of the cylindrical lithium-ion battery at different SoCs under -20℃

Table 9 R_s, R_p, C_p, and L_s (-20℃)

Division	-20℃
100% SoC	R_s = 23.4937 mΩ, R_p = 252.3713 mΩ C_p = 0.5820 F, L_s = 3.7391 mH
50% SoC	R_s = 23.9596 mΩ, R_p = 386.7496 mΩ C_p = 0.6367 F, L_s = 3.6541 mH
0% SoC	R_s = 25.2552 mΩ, R_p = 874.5938 mΩ C_p = 1.7687 F, L_s = 4.0195 mH

4. Conclusion

This study examined the influence of temperature and SoC on the diffusion area's EIS properties in a cylindrical lithium-ion battery.

The change in the diffusion area with decreasing temperature from 40℃ to -20℃ was as follows.

At high SoC levels (100% and 50%), the diffusion behavior followed the sequence: WD → SSD → BD. At 0% SoC, the pattern shifted from WD to SCD.

As SoC decreased from 100% to 0%, the diffusion mode also changed depending on temperature. At 40℃, 25℃, and 10℃, WD was maintained. At -5℃, the transition occurred from SSD to SCD, while at -20℃, it shifted from BD to SCD.

Furthermore, the results showed that the performance of cylindrical lithium-ion batteries deteriorated under low-frequency diffusion at 0 Hz and that the diffusion phenomena manifests differently depending on the battery's SoC and ambient temperature.

The low-frequency diffusion region observed in the impedance spectra of the cylindrical lithium-ion battery demonstrated a progressive transition in diffusion behavior depending on both temperature and SoC. Specifically, the diffusion mode followed the sequential order of WD, SSD, BD, and finally, SCD.

Author contributions

J. Y. Bae ; Conceptualization, Investigation, Data curation, Formal analysis, Methodology, Validation, Writing-original draft, Writing-review & editing.

References

1. P. Sun, R. Bisschop, H. Niu and X. Huang, 2020, "A Review of Battery Fires in Electric Vehicles", Fire Technology, 56, 1361-1410. (DOI:10.1007/s10694-019-00944-3)
2. L. Komsiyska, T. Buchberger, S. Diehl, M. Ehrensberger, C. Hanzl, C. Hartmann, M.

Hölzle, J. Kleiner, M. Lewerenz, B. Liebhart, M. Schmid, D. Schneider, S. Speer, J. Stöttner, C. Terbrack, M. Hinterberger and C. Endisch, 2021, “Critical Review of Intelligent Battery Systems: Challenges, Implementation, and Potential for Electric Vehicles”, Energies, 14(5989), 1-82.
(DOI:10.3390/en14185989)

3. E. T. Sayed, A. G. Olabi, A. H. Alami, A. Radwan, A. Mdallal, A. Rezk and M. A. Abdelkareem, 2023, “Renewable Energy and Energy Storage Systems”, Energies, 16(1415), 1-26.
(DOI:10.3390/en16031415)
4. B. K. Sovacool, 2009, “The importance of comprehensiveness in renewable electricity and energy-efficiency policy”, Energy Policy, 37, 1529-1541.
(DOI:10.1016/j.enpol.2008.12.016)
5. S. Li, C. C. Mi and M. Zhang, 2013, “A High-Efficiency Active Battery-Balancing Circuit Using Multi-winding Transformer”, IEEE Transactions on Industry Applications, 49(1), 198-207.
(DOI:10.1109/TIA.2012.2229455)
6. T. N. V. Krishna, S. V. S. V. P. D. Kumar, S. S. Rao and L. Chang, 2024, “Powering the Future: Advanced Battery Management Systems (BMS) for Electric Vehicles”, Energies, 17 (3360), 1-18.
(DOI:10.3390/en17143360)
7. J. Li, D. Sun, X. Jin, W. Shi and C. Sun, 2019, “Lithium-ion Battery Overcharging Thermal Characteristics Analysis and an Impedance-Based Electro-Thermal Coupled Model Simulation”, Applied Energy, 254(113574), 1-12.
(DOI:10.1016/j.apenergy.2019.113574)
8. P. Peng and F. Jiang, 2016, “Thermal Safety of Lithium-ion Batteries with Various Cathode Materials: A Numerical Study”, International Journal of Heat and Mass Transfer, 103, 1008-1016.
(DOI:10.1016/j.ijheatmasstransfer.2016.07.088)
9. J. Kleiner, L. Komsiyska, G. Elger and C. Endisch, 2020, “Thermal Modelling of a Prismatic Lithium-Ion Cell in a Battery Electric Vehicle Environment: Influences of the Experimental Validation Setup”, Energies, 13(62), 1-18.
(DOI:10.3390/en13010062)
10. E. Karden, S. Buller and R. W. D. Doncker, 2002, “A Frequency-domain Approach to Dynamical Modeling of Electrochemical Power Sources”, Electrochimica Acta, 47, 2347-2356.
(DOI:10.1016/S0013-4686(02)00091-9)
11. M. Oldenburger, B. Bedürftig, A. Gruhle, F. Grimsmann, E. Richter, R. Findeisen and A. Hintennach, 2019, “Investigation of the low frequency warburg impedance of li-ion cells by frequency domain measurements”, Journal of Energy Storage, 21, 272-280.
(DOI:10.1016/j.est.2018.11.029)